Preparation of Perovskite Films under Liquid Nitrogen Atmosphere for High Efficiency Perovskite Solar Cells

*Putao Zhang, Fu Yang, Gaurav Kapil, Chi Huey Ng, Tingli Ma, and Shuzi Hayase**

Kyushu Institute of Technology, 2-4 Hibikino, Wakamatsu-ku, Kitakyushu, 808-0196, Japan

Abstract: High quality perovskite film with high coverage and tight grain arrangement is key factor for obtaining high performance and stable perovskite devices. Herein, high quality perovskite films were successfully prepared by liquid nitrogen assisted method (LN method). Here, the vaporization of liquid nitrogen reduces the ambient temperature and absorb thermal energy from the substrate surface to increase the nucleation speed of perovskite. The scanning electron microscopy results showed that $CH_3NH_3PbI_3$ perovskite films prepared by liquid nitrogen assisted method were dense and pinhole-free. The devices prepared by the LN method results to a high-performance with the power conversion efficiency (PCE) up to 16.53%, and the performance could maintain more than 89% of the primary PCE after 30 days storage in a desiccator at room temperature.
Keywords: Nucleation, Perovskite solar cell, High quality perovskite film, Liquid nitrogen, Trap, Grain boundaries

Introduction

In recent few years, perovskite solar cells (PSCs) have gained great attention owing to the long diffusion length, suitable band gap, and of the superior carrier mobility perovskite materials.[1-2] Miyasaka research group first reported the efficiency of 3.8% liquid-electrolyte-based PSCs in 2009,[3] which within a few short years reached an efficiency over 23%.[4] The key factor for getting high performance PSCs is to control the morphology for getting high quality of perovskite layer. Various preparation ways or deposition techniques are introduced to prepare high-quality perovskite films, such as interface engineering,[5] solvent engineering,[6-7] composition modulation[8-9] and so on.[10-14] All of these methods are based on crystal nucleation-growth theory to control the morphology of the film.[15-17] According to the crystal nucleation-growth theory and previous reports, rapid nucleation and slow growth are the key factors for obtaining dense and smooth perovskite films.[18-19] In an one-step anti-solvent method, Dai et al.[20] have reported the method to enhance the perovskite films` quality through lowering the anti-solvent`s temperature. The low-temperature anti-solvent not only removes the excess solvent from the perovskite precursor solution to increase the precursor concentration, but also lowers the temperature on the substrate, allowing the perovskite precursor film to reach super-cooling quickly, thereby facilitating rapid nucleation. By this method they have improved the surface coverage of perovskite layer. Furthermore, the speed of crystal growth is also playing an important role for the film. If the grain growth is too fast, it will lead to a film with high defect density.[21] Zhu et al. has experimentally added $MAPbCl_3$ to the perovskite precursor.[22] In this case the crystal growth rate is effectively reduced, and a well-formed perovskite film is obtained. However, preparation of high-coverage and low-defect perovskite films still poses great challenges. In this study, a liquid nitrogen assisted one-step anti-solvent process was used to prepare perovskite films. The volatile liquid nitrogen takes away the heat from the perovskite precursor film,

accelerating the rapid nucleation process of the perovskite. Through this process, a pinhole-free smooth and dense perovskite film was obtained. The average PCE of the regular mesoporous structure devices by incorporating these high-quality perovskite films significantly improved from the initial 14.50% to 15.54% and the champion device in this work shows the highest PCE of 16.53%. 89% of the initial performance was retained even after 30 days of cell fabrication.

Results and discussion

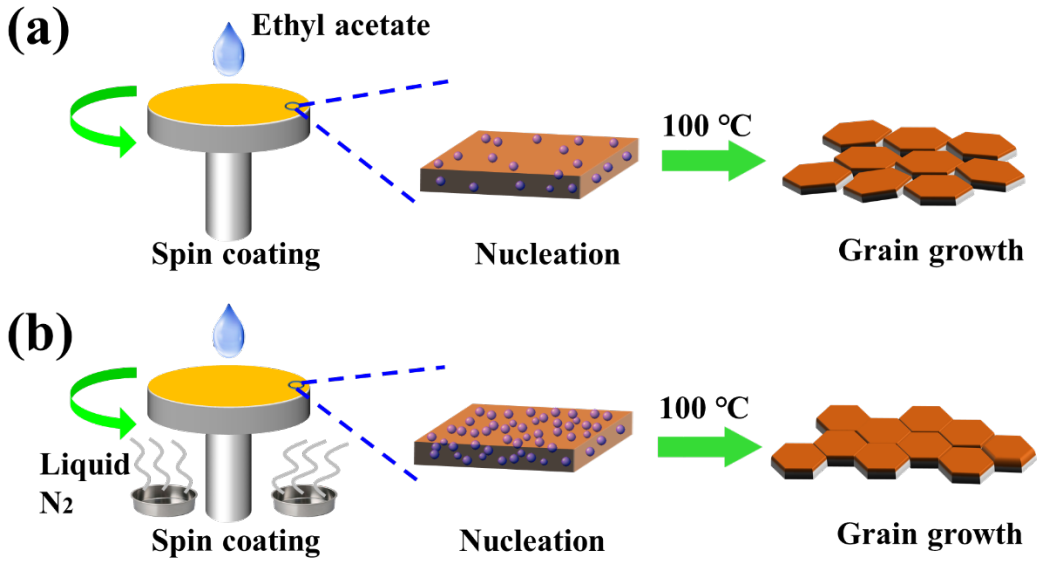

Fig. 1. Fabricating perovskite films method of conventional one-step spin-coating process (a) and liquid nitrogen assisted process (b). Conventional one-step spin-coating method usually results in rich defects at a grain boundary, where non-uniform large crystals from a result of slow nucleation. In the liquid nitrogen assisted method (NL method), perovskite precursor solution can easily reach below the degree of undercooling, and rapidly and massively nucleate, thereby forming densely arranged grains of film.

The one-step spin-coating anti-solvent method for preparing the $CH_3NH_3PbI_3$ layer is shown in Fig. 1. In the conventional process (a), a perovskite precursor solution was spin-coated on the TiO_2 substrate at 4000 rpm. After a delay time for 10 s, ethyl acetate anti-solvent was dripped on the substrates. The anti-solvent reduces the solubility of perovskite in the precursor film, promoting growth of the crystals and fast nucleation in the film. After annealed at 100 ℃ on a hot plate for 10 min to evaporate the residual solvent and further promote crystal growth, the perovskite film was achieved. While in the liquid nitrogen assist process (b), liquid nitrogen is used as an aid, as shown in Fig. S3, two stainless steel petri dishes filled with liquid nitrogen were placed under the spinner. It is noted that the spin-coating instrument accelerates the volatilization of liquid nitrogen during high-speed rotation. Therefore, sufficient liquid nitrogen should be injected into the stainless steel petri dishes before spin coating to ensure continuous liquid nitrogen volatilization during spin coating. The low-temperature nitrogen evaporated from liquid N_2 allows the perovskite to nucleate rapidly on the precursor film. The crystal grows after baking to form a dense perovskite film. According to the previous reports, during the preparation

of perovskite film, the slow nucleation leads to large grain boundaries and poor film coverage in the films.[18, 23] To solve this problem, researchers have tried to improve the film preparation by different anti-solvents.[24] The anti-solvent allows the initial solution to quickly reach supersaturation, which in turn promotes nucleation. As is well known, the key factors affecting crystal nucleation are supersaturation and undercooling. In this study, the liquid nitrogen assisted process effectively reduces the surface temperature of the precursor film to reach the nucleation critical state, and promoting a large number of nucleation in a short time.

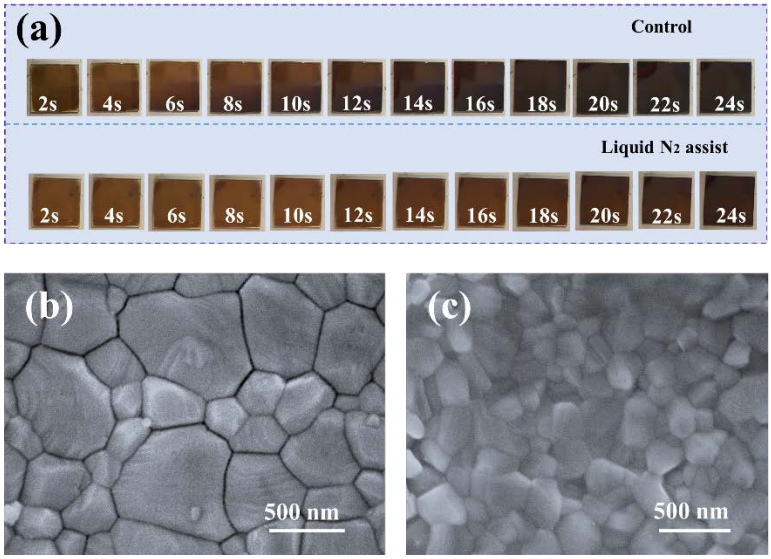

Fig. 2. (a) Photographs of perovskite $CH_3NH_3PbI_3$ films during annealing process at 100 °C. Top-view SEM images of $CH_3NH_3PbI_3$ layers deposited on TiO_2/FTO: (b) control, (c) LN method.

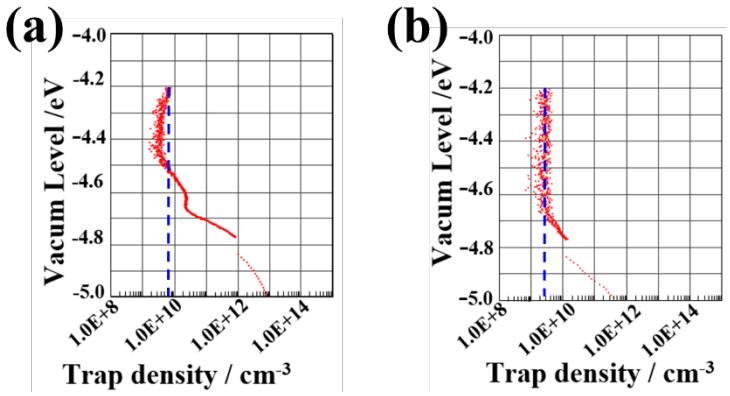

Fig. 3 Trap distribution on perovskite films. (a) Control and (b) LN method.

Fig. 2 (a) presents a comparison of perovskite films prepared by conventional processes and LN process. Compared with the controlled group, the perovskite film prepared by LN method took a longer time to complete the crystallization process, resulting in high quality morphology densely packed grains in the perovskite films. The top-view SEM images of the $CH_3NH_3PbI_3$ layers are

illustrated in Fig. 2b-c. As can be seen in Fig. 2b, the perovskite films with big grains and significant grain boundary defects are formed by the conventional process. In general, a perovskite film with a large crystal is more advantageous for charge transport, but due to a large number of grain boundary defects, the performance of the device is not ideal.[25] Large grain boundary defects might cause direct contact between the electron transporting layer and the hole transporting layer, which cause charge leakage and non-radiative recombination.[26] However, as shown in Fig. 2c, a close-grained perovskite film can be obtained by a liquid nitrogen assist method. The grains of this dense perovskite film were almost linked together without large gap between grains, which reduces the carrier's non-radiative recombination and promotes the efficient transmission of charges in the device.[27] Thermally stimulated current (TSC) was introduced to explore the trap density of $CH_3NH_3PbI_3$ layers. TSC is a powerful measuring tool to investigate the trap distribution of the trapped charge carriers within the perovskite material. Generally, the carrier traps are priorly cooled to the temperature of liquid nitrogen, followed by the filling of carriers generated from the electrodes under a small forward bias. The trapped carries are subsequently released and obtained through slowly rising up the temperature at a continuous speed of 2 ºC/min under a small reverse bias, which gives rise to the TSC curves.[28] The results are shown in Fig. 3. The conduction band level of $CH_3NH_3PbI_3$ is -3.93 eV from vacuum level, for control group trap density at -4.2 eV was $5\times10^9/cm^3$, as shown in Fig. 3a. While, trap density of perovskite film prepared by LN method decreased significantly, was about was $2\times10^9/cm^3$ at the same level (see Fig. 3b).

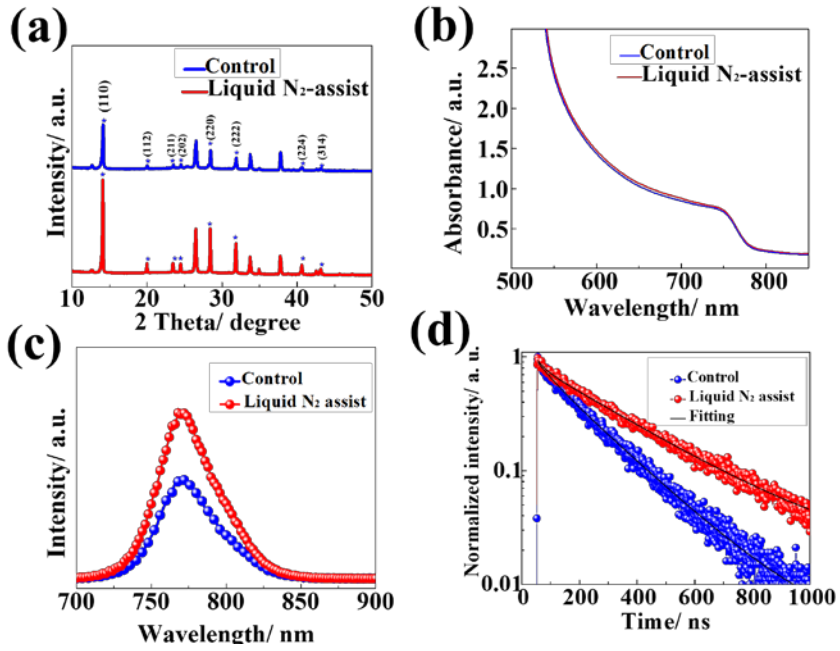

Fig. 4. (a) X-ray diffraction spectra and (b) Ultraviolet–visible spectroscopy absorption spectra of $CH_3NH_3PbI_3$ layers prepared on TiO_2 with or without liquid nitrogen assistance. (c) PL spectra and (d) TRPL spectra of the glass/$CH_3NH_3PbI_3$ films.

The crystalline properties of perovskite films were further recorded by XRD. As shown in Fig. 4a, the X-ray patterns of perovskite layers prepared with or without liquid nitrogen assistance displayed typical diffraction peaks of $CH_3NH_3PbI_3$ perovskite phase. The diffraction peaks at 14.17, 20.04, 23.59, 24.56, 28.52, 31.94, 40.55 and 43.22°, can be assigned to the (110), (112), (211), (202), (220), (222), (224) and (314) planes of the tetragonal $CH_3NH_3PbI_3$ structure.[29] The intensity of

the perovskite peaks (red) was significantly enhanced and full width at half maximum (FWHM) was narrow than that of control (see Fig. S4). This suggests film crystallinity prepared by the LN method is better than that of control. The good crystallinity of perovskite film led to good optical properties. As shown in Fig. 4b, the perovskite film prepared by LN method showed almost the same absorption. The high-quality perovskite film as described above can transport carriers more effectively and effectively reduce charge recombination as well. Next, the steady-state photoluminescence (PL) and time-resolved photoluminescence (TRPL) test were performed on the perovskite film. The results are shown in Fig. 4c and d. Compared with the control group, it can be found that the PL peak of the film prepared by LN process was stronger. This means that the film prepared by the LN method has a higher quality. The TRPL results are shown in Fig. 4d. The film prepared by LN process had a carrier lifetime of 61.2 ns, which is much longer than that of the control group (27.9 ns). Therefore, the LN method effectively increased the carrier lifetime of perovskite films, which is agreed with the photoluminescence spectra.

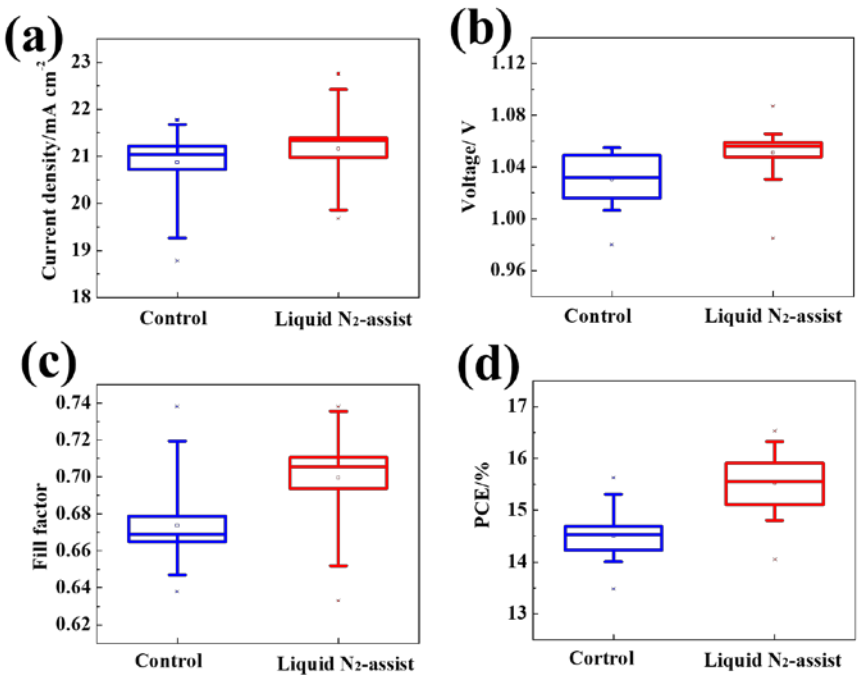

Fig. 5. Photovoltaic statistics of two group perovskite solar cells. (a) J_{SC}, (b) V_{OC}, (c) FF, (d) PCE. Statistical analysis of data from 30 cells of each group.

Fig. 5 (a-d) show the photovoltaic statistics of two group perovskite solar cells with the structure FTO/c-TiO_2/m-TiO_2/$MAPbI_3$/HTL/Au. The devices parameters showed that the LN method can effectively improve all the photovoltaic parameters of PSCs including J_{SC}, V_{OC} and FF. The schematic of device structure and cross-section SEM image of the completed devices, as shown in Fig. 6a-b. As mentioned above, the closely arranged grain and high-quality perovskite films prepared by the LN method result in higher J_{SC}. In addition, fewer grain boundary pinholes can effectively avoid contact between hole transporting layer and electron transporting layer (see Fig. 6c-d), which can reduce electric leakage, and reduce carrier recombination, improving both V_{OC} and FF.[30]

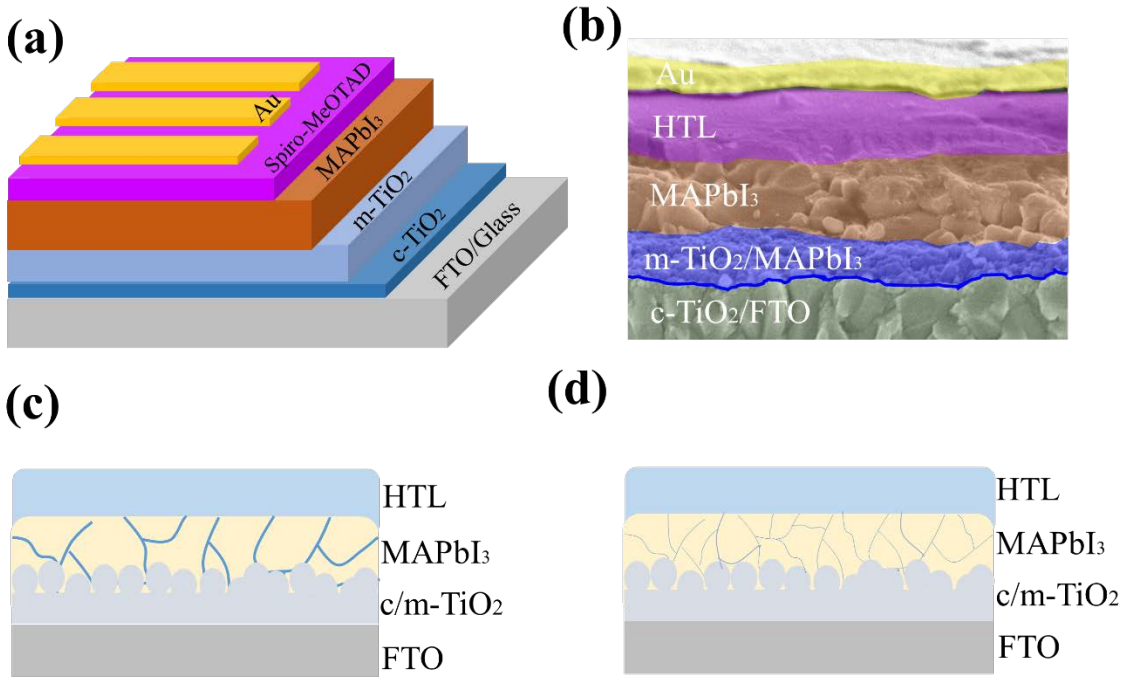

Fig. 6 (a) Device structure of FTO/c-TiO_2/m-TiO_2/$MAPbI_3$/HTL/Au PSCs and (b) cross-section SEM image of the completed devices. Cross sectional structure of perovskite film prepared by (c) conventional process with large grain boundary pin holes and (d) LN method with small grain boundary defects.

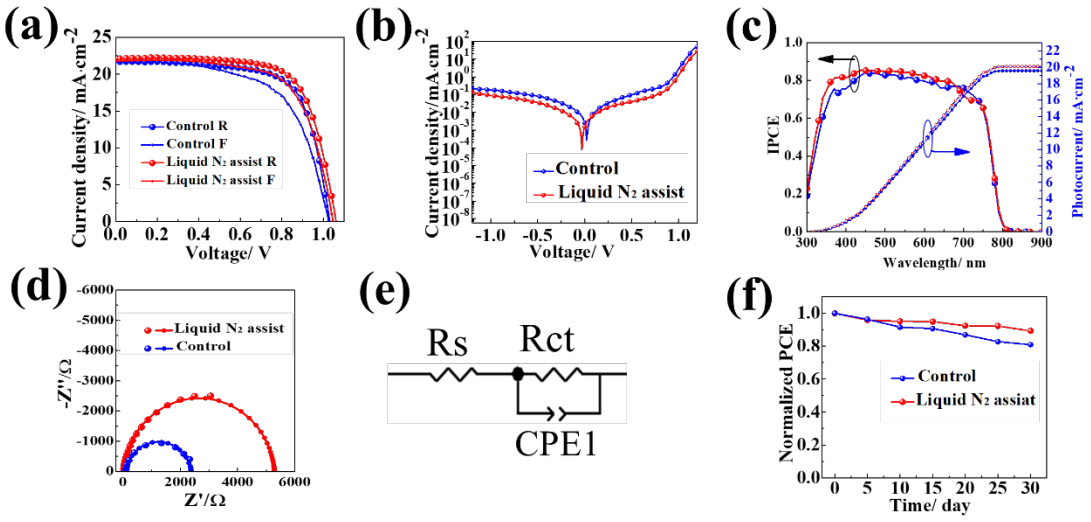

Fig. 7 The illuminated (a) and dark (b) Current-voltage characteristics and (c) EQE spectra of the champion PSCs based conventional method and LN method. (d) Nyquist plots of PSCs

measured with an applied bias of 0.6 V in dark condition and (e) an equivalent circuit. (f) Stability test for control and liquid nitrogen assisted perovskite solar cells.

Fig. 7 (a) illustrates the J-V characteristics of champion PSCs prepared using conventional way and LN method, tested under reverse and forward voltage. The device prepared by conventional method (blue curve) achieved a PCE of 15.63 (13.66) %, with a V_{OC} of 1.03 (1.02) V, J_{SC} of 21.69 (21.68) mA·cm^{-2}, and FF of 0.70 (0.62) measured under reverse (forward) direction, showing a large hysteresis. While the device prepared by LN method (red curve) achieved a PCE of 16.53 (15.71) %, with a V_{OC} of 1.06 (1.05) V, a J_{SC} of 22.19 (21.77) mA·cm^{-2} and a FF of 0.70 (0.69) measured under reverse (forward) direction, revealing a decreased hysteresis and an enhanced efficiency. Due to the excellent quality $CH_3NH_3PbI_3$ layer prepared by the LN method, there are no pinholes, and less grain boundary defects, which reduces the carrier recombination sites and reduces the hysteresis. The PCE enhancement is mainly attributed to the improvement in J_{SC} and V_{OC}. The high quality film with less grain boundary pin holes will reduce the shunt pathways and effectively block electrons on the $TiO_2/CH_3NH_3PbI_3$ interface to decrease electron-hole recombination (see Fig. 6a, b). It can also be seen in the dark current curve (Fig. 7 b), that the dark current of the LN device was lower than that of the control device, thereby leading to a larger V_{OC} of the device prepared by liquid nitrogen assisted method.[31] Fig. 7 (c) shows the IPCE spectra of the champion devices. The integrated current densities were 20.10 and 19.58 mA·cm^{-2} for control and liquid nitrogen assisted devices, respectively. Electrochemical impedance spectrum (EIS) is an effective method to study the charge recombination in devices. Fig. 7 (d) presents the Nyquist plots of both devices carried out in the dark condition at an applied voltage of 0.6 V. The series resistance (Rs) and charge recombination resistance (R_{ct}) could be fitted by employing an equivalent circuit model (Fig. 7 e), in the equivalent circuit model.[32] As a result, the device prepared by liquid nitrogen assisted method has an R_{ct} of 5276 Ω, which is higher than conventional devices (2293 Ω), suggesting that electron recombination can be effectively reduced. The Nyquist plots measured with different applied bias are displayed in Fig. S5 a-b. According to the equivalent circuit model the corresponding results were plotted as shown in Fig S5 c. It can be seen that at the same applied bias, the LN group has a higher R_{ct}, which could explain the higher V_{OC} achieved from the current voltage measurements.[33] We examined the long-term stability of the PSCs. The stability measurement of the unencapsulated PSCs were performed in a desiccator with 20-40% humidity at room temperature for 30 days. As shown in Fig. 7 (f), device prepared by the LN method showed a better stability, maintaining 89% of the initial PCE after 30 days of storage in desiccator, whereas the control group drop more of the initial efficiency under the same conditions.

Conclusions

In summary, we introduced an efficient and facile approach to prepare high quality perovskite film. During the process of perovskite nucleation, the LN method effectively reduces the ambient temperature, taking away heat from the substrate surface and accelerating the nucleation process. By observing the film morphology, we found that the LN method can produce pinhole-free, grain tightly arranged perovskite films. At last, an effective PCE of 16.53% was observed for the film prepared by the LN method. The performance could retain over 89% of the initial PCE after 30 days storage in 20-40% humidity air condition at room temperature.

Supporting Information.

Additional data and results

Acknowledgments

This work was supported by China Scholarship Council (CSC) (No. 201608210184), Core Research for Evolutional Science and Technology (CREST) project of Japan Science and Technology (JST).

Corresponding Author

* Email: hayase@life.kyutech.ac.jp.

Reference

(1) Bi, C.; Wang, Q.; Shao, Y.; Yuan, Y.; Xiao, Z.; Huang, J. Non-wetting surface-driven high-aspect-ratio crystalline grain growth for efficient hybrid perovskite solar cells. *Nature communications* **2015,** *6*, 7747.
(2) Yang, F.; Kamarudin, M. A.; Zhang, P.; Kapil, G.; Ma, T.; Hayase, S. Enhanced crystallization by methanol additive in anti-solvent for achieving high- quality $MAPbI_3$ perovskite films in humid atmosphere. *ChemSusChem* **2018**, *11*, 2265-2265.
(3) Kojima, A.; Teshima, K.; Shirai, Y.; Miyasaka, T. Organometal halide perovskites as visible-light sensitizers for photovoltaic cells. *J. Am. Chem. Soc.* **2009,** *131*, 6050-6051.
(4) Jeon, N. J.; Na, H.; Jung, E. H.; Yang, T.-Y.; Lee, Y. G.; Kim, G.; Shin, H.-W.; Seok, S. I.; Lee, J.; Seo, J. A fluorene-terminated hole-transporting material for highly efficient and stable perovskite solar cells. *Nature Energy* **2018**, *3*, 682-689.
(5) Huang, L.-B.; Su, P.-Y.; Liu, J.-M.; Huang, J.-F.; Chen, Y.-F.; Qin, S.; Guo, J.; Xu, Y.-W.; Su, C.-Y. Interface engineering of perovskite solar cells with multifunctional polymer interlayer toward improved performance and stability. *J. Power Sources* **2018,** *378*, 483-490.
(6) Kim, Y. Y.; Park, E. Y.; Yang, T.-Y.; Noh, J. H.; Shin, T. J.; Jeon, N. J.; Seo, J. Fast two-step deposition of perovskite via mediator extraction treatment for large-area, high-performance perovskite solar cells. *Journal of Materials Chemistry A* **2018**, *6*, 12447-12454.
(7) Tu, Y.; Wu, J.; He, X.; Guo, P.; Wu, T.; Luo, H.; Liu, Q.; Wang, K.; Lin, J.; Huang, M. Solvent engineering for forming stonehenge-like PbI_2 nano-structures towards efficient perovskite solar cells. *Journal of Materials Chemistry A* **2017,** *5*, 4376-4383.
(8) Kim, J.; Saidaminov, M. I.; Tan, H.; Zhao, Y.; Kim, Y.; Choi, J.; Jo, J. W.; Fan, J.; Quintero-Bermudez, R.; Yang, Z. Amide- catalyzed phase- selective crystallization reduces defect density in wide-bandgap perovskites. *Adv. Mater.* **2018,** *30*, 1706275.
(9) Tombe, S.; Adam, G.; Heilbrunner, H.; Yumusak, C.; Apaydin, D. H.; Hailegnaw, B.; Ulbricht, C.; Arendse, C. J.; Langhals, H.; Iwuohaa, E. The influence of perovskite precursor composition on the morphology and photovoltaic performance of mixed halide $MAPbI_{3-x}Cl_x$ solar cells. *Solar Energy* **2018,** *163*, 215-223.
(10) Dong, H.; Wu, Z.; Xi, J.; Xu, X.; Zuo, L.; Lei, T.; Zhao, X.; Zhang, L.; Hou, X.; Jen, A. K. Y. Pseudohalide-induced recrystallization engineering for $CH_3NH_3PbI_3$ film and its application

in highly efficient inverted planar heterojunction perovskite solar cells. *Adv. Funct. Mater.* **2018,** *28*, 1704836.
(11) Li, Y.; Li, Y.; Shi, J.; Zhang, H.; Wu, J.; Li, D.; Luo, Y.; Wu, H.; Meng, Q. High quality perovskite crystals for efficient film photodetectors induced by hydrolytic insulating oxide substrates. *Adv. Funct. Mater.* **2018**.*10*, 1705220.
(12) Fu, X.; Dong, N.; Lian, G.; Lv, S.; Zhao, T.; Wang, Q.; Cui, D.; Wong, C.-P. High-quality $CH_3NH_3PbI_3$ films obtained via a pressure-assisted space-confined solvent-engineering strategy for ultrasensitive photodetectors. *Nano Lett.* **2018,** *18*, 1213-1220.
(13) Jiang, Y.; Tu, L.; Li, H.; Li, S.; Yang, S.-E.; Chen, Y. A feasible and effective post-treatment method for high-quality $CH_3NH_3PbI_3$ films and high-efficiency perovskite solar cells. *Crystals* **2018,** *8*, 44.
(14) Ito, N.; Kamarudin, M. A.; Hirotani, D.; Zhang, Y.; Shen, Q.; Ogomi, Y.; Iikubo, S.; Minemoto, T.; Yoshino, K.; Hayase, S. Mixed Sn-Ge perovskite for enhanced perovskite solar cell performance in air. *The journal of physical chemistry letters* **2018,** *9*, 1682-1688.
(15) LaMer, V. K.; Dinegar, R. H. Theory, production and mechanism of formation of monodispersed hydrosols. *J. Am. Chem. Soc.* **1950,** *72*, 4847-4854.
(16) Wang, F.; Richards, V. N.; Shields, S. P.; Buhro, W. E. Kinetics and mechanisms of aggregative nanocrystal growth. *Chem. Mater.* **2013,** *26*, 5-21.
(17) Luo, W.; Wu, C.; Sun, W.; Guo, X.; Xiao, L.; Chen, Z. High crystallization of perovskite film by a fast electric current annealing process. *ACS applied materials & interfaces* **2017,** *9*, 26915-26920.
(18) Qin, P. L.; Yang, G.; Ren, Z. w.; Cheung, S. H.; So, S. K.; Chen, L.; Hao, J.; Hou, J.; Li, G. Stable and efficient organo-metal halide hybrid perovskite solar cells via π-conjugated lewis base polymer induced trap passivation and charge extraction. *Adv. Mater.* **2018,** *30*, 1706126.
(19) Zhang, F.; Shi, W.; Luo, J.; Pellet, N.; Yi, C.; Li, X.; Zhao, X.; Dennis, T. J. S.; Li, X.; Wang, S. Isomer-pure bis-PCBM-assisted crystal engineering of perovskite solar cells showing excellent efficiency and stability. *Adv. Mater.* **2017,** *29*, 1606806.
(20) Ren, Y.-K.; Ding, X.-H.; Wu, Y.-H.; Zhu, J.; Hayat, T.; Alsaedi, A.; Xu, Y.-F.; Li, Z.-Q.; Yang, S.-F.; Dai, S.-Y. Temperature-assisted rapid nucleation: A facile method to optimize the film morphology for perovskite solar cells. *Journal of Materials Chemistry A* **2017,** *5*, 20327-20333.
(21) Bai, S.; Sakai, N.; Zhang, W.; Wang, Z.; Wang, J. T.-W.; Gao, F.; Snaith, H. J. Reproducible planar heterojunction solar cells based on one-step solution-processed methylammonium lead halide perovskites. *Chem. Mater.* **2016,** *29*, 462-473.
(22) Zhao, Y.; Zhu, K. CH_3NH_3Cl-assisted one-step solution growth of $CH_3NH_3PbI_3$: Structure, charge-carrier dynamics, and photovoltaic properties of perovskite solar cells. *The Journal of Physical Chemistry C* **2014,** *118*, 9412-9418.
(23) Hao, J.; Hao, H.; Cheng, F.; Li, J.; Zhang, H.; Dong, J.; Xing, J.; Liu, H.; Wu, J. Improved performance of mesostructured perovskite solar cells via an anti-solvent method. *J. Cryst. Growth* **2018,** *491*, 66-72.
(24) Yang, F.; Kapil, G.; Zhang, P.; Hu, Z.; Kamarudin, M. A.; Ma, T.; Hayase, S. Dependence of acetate-based antisolvents for high humidity fabrication of $CH_3NH_3PbI_3$ perovskite devices in ambient atmosphere. *ACS applied materials & interfaces* **2018**.*10*, 16482-16489.
(25) Yang, M.; Zhang, T.; Schulz, P.; Li, Z.; Li, G.; Kim, D. H.; Guo, N.; Berry, J. J.; Zhu, K.; Zhao, Y. Facile fabrication of large-grain $CH_3NH_3PbI_{3-x}Br_x$ films for high-efficiency solar cells via CH_3NH_3Br-selective ostwald ripening. *Nature communications* **2016,** *7*, 12305.

(26) Long, R.; Liu, J.; Prezhdo, O. V. Unravelling the effects of grain boundary and chemical doping on electron-hole recombination in $CH_3NH_3PbI_3$ perovskite by time-domain atomistic simulation. *J. Am. Chem. Soc.* **2016,** *138*, 3884-3890.
(27) Ng, A.; Ren, Z.; Li, G.; Djurišic, A. B.; Surya, C. Novel growth techniques for the deposition of high-quality perovskite thin films. *Oxide-based Materials and Devices IX, International Society for Optics and Photonics*. **2018**; *10533*, 105331Y.
(28) Qin, C.; Matsushima, T.; Fujihara, T.; Potscavage Jr, W. J.; Adachi, C. Degradation mechanisms of solution-processed planar perovskite solar cells: Thermally stimulated current measurement for analysis of carrier traps. *Adv. Mater.* **2016,** *28*, 466-471.
(29) Yu, J.; Chen, X.; Wang, Y.; Zhou, H.; Xue, M.; Xu, Y.; Li, Z.; Ye, C.; Zhang, J.; Van Aken, P. A. A high-performance self-powered broadband photodetector based on a $CH_3NH_3PbI_3$ perovskite/ZnO nanorod array heterostructure. *Journal of Materials Chemistry C* **2016,** *4*, 7302-7308.
(30) Cho, K. T.; Paek, S.; Grancini, G.; Roldán-Carmona, C.; Gao, P.; Lee, Y.; Nazeeruddin, M. K. Highly efficient perovskite solar cells with a compositionally engineered perovskite/hole transporting material interface. *Energy & Environmental Science* **2017,** *10*, 621-627.
(31) Jhuo, H.-J.; Yeh, P.-N.; Liao, S.-H.; Li, Y.-L.; Sharma, S.; Chen, S.-A. Inverted perovskite solar cells with inserted cross-linked electron-blocking interlayers for performance enhancement. *Journal of Materials Chemistry A* **2015,** *3*, 9291-9297.
(32) Jiang, L.-L.; Cong, S.; Lou, Y.-H.; Yi, Q.-H.; Zhu, J.-T.; Ma, H.; Zou, G.-F. Interface engineering toward enhanced efficiency of planar perovskite solar cells. *Journal of Materials Chemistry A* **2016,** *4*, 217-222.
(33) Jiang, X.; Yu, Z.; Zhang, Y.; Lai, J.; Li, J.; Gurzadyan, G. G.; Yang, X.; Sun, L. High-performance regular perovskite solar cells employing low-cost poly (ethylenedioxythiophene) as a hole-transporting material. *Scientific reports* **2017,** *7*, 42564.

Abstract Graphic

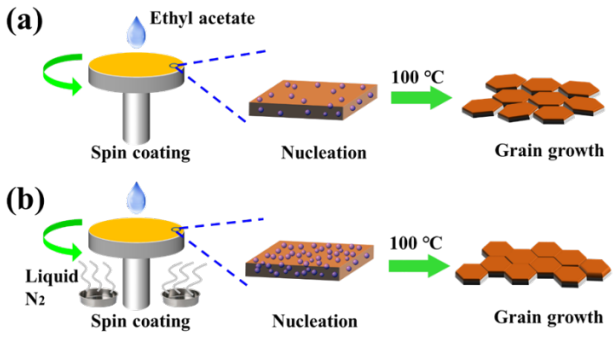

A new energy-saving idea to fabricate the highly stable and efficient perovskite solar cell in the environment of Nitrogen fumes (For Table of Contents Use Only).

Cover sheet-Supporting Information

Manuscript title: "Preparation of Perovskite Films under Liquid Nitrogen Atmosphere for High Efficiency Perovskite Solar Cells"
List of authors: Putao Zhang, Fu Yang, Gaurav Kapil, Chi Huey Ng, Tingli Ma, and Shuzi Hayase *

Number of pages: 9 pages (including the cover sheet)

Number of figures: 5 figures

Number of tables: 2 tables

Electronic Supplementary Information for

Preparation of Perovskite Films under Liquid Nitrogen Atmosphere for High Efficiency Perovskite Solar Cells

Experimental Section

Materials. Unless specified otherwise, all materials were purchased from either Wako or TCI and used as received.

Device fabrication.

Substrate preparation: Firstly, fluorine doped tin oxide substrates (FTO-coated glass) (Nippon Sheet Glass Co. Ltd.) were cut into squares with dimensions of 20 × 20 mm^2 and etched with Zn powder and HCl aqueous (6 M). Then the substrates were washed by ultrasonication with diluted detergent, (10% in water), isopropanol, acetone and deionized water for 20 min, respectively. A 30~50 nm-thick compact layer of TiO_2 (c-TiO_2) was then coated on the substrates by spin coating of a 0.15 mM bis(isopropoxide)bis(acetylacetonato)titanium(IV) solution (75% in 2-propanol, Sigma-Aldrich) in 1-butanol at 2000 rpm for 20 s and then baked on the hotplate at 125 °C for 5 min (thickness of the c-TiO_2 is about 40 nm in this work, see Fig. S1 in supporting information). After cooling down to room temperature, the diluted-TiO_2 paste (30 NRD/ethanol = 1/ 4, weight ratio) was spin-coated on the c-TiO_2 layer at 5000 rpm for 30 s, followed by drying on a hotplate at 125 °C for 10 min, then annealing at 500 °C for 1 h to provide a 150~200 nm-thick mesoporous TiO_2 (m-TiO_2) (in this work thickness of the m-TiO_2 is about 174 nm, see Fig. S2).

Perovskite precursor solution and film deposition: Perovskite layer, $CH_3NH_3PbI_3$, was formed using one-step anti-solvent method. Perovskite precursor solutions with a concentrations of 1.5 M were prepared by dissolving Methylammonium iodide (MAI) and lead iodide (PbI_2) (MAI/PbI_2 = 1:1.05, molar ratio) in a mixture solution of N, N-dimethylformide (DMF) and dimethyl sulfoxide (DMSO) (DMF/DMSO = 4/1, volume ratio) and stirring at room temperature for 1 hour. To prepare light harvesting layer, the perovskite solution (50 μL) was first dropped onto a TiO_2/FTO substrate. The substrate was then spun at 4000 rpm for 25 s, and during the 10^{th} seconds 500 μL of anhydrous ethyl acetate was quickly dropped on the spinning substrate. The obtained films were then annealed at 100 °C for 10 min in air environment. For the preparation of perovskite film by LN method, as shown in Fig. S3 b, two stainless steel petri dishes (5cm in diameter and 1.5cm in depth) filled with liquid nitrogen (~ 20 mL) were placed under the spinner before spin coating.

Hole transporting layer and Au electrode: A 50 μL of Spiro-OMeTAD solution was spin-coated on the top of perovskite layer at 4000 rpm for 30 s. The Spiro-OMeTAD solution was prepared by dissolving 72.3 mg of Spiro-OMeTAD in 1 mL of chlorobenzene, to which 28.8 μL

of 4-tert-butyl pyridine (4-tBP) and 17.5 μL of lithium bis(trifluoromethanesulfonyl)imide (Li-TFSI) (520 mg LI-TSFI in 1 mL acetonitrile) were added. Finally, an 80-nm-thick of Au was thermally evaporated on the Spiro-OMeTAD-coated film. Note that the samples were left in a desiccator overnight before the gold electrode was prepared.

Film and device characterization

The thickness of the TiO_2 layer were measured using a Veeco Dektak 150 surface profilometer. A field-emission scanning electron microscope (FE-SEM, Jeol JSM 6700F) was used to investigate the morphology of the perovskite film top view and the device cross section. Absorption spectral measurements were recorded using Shimadzu UV-2550 UV-visible spectrophotometer. A solar simulator (KHP-1, Bunko-Keiki, Japan) fitted with a filtered 1000 W xenon lamp was used to provide simulated solar irradiation (AM1.5, 100 $mW \cdot cm^{-2}$). Illumination intensity of the solar simulator was confirmed by a standard silicon reference cell (BS-520 S/N 007, Bunko-Keiki, Japan). Current-voltage (J-V) characteristics were measured using a Keithley 2400 source meter. The solar cells were masked with a non-reflective metal aperture of 0.1 cm^2 to define the working area of the device and avoid light scattering through the edges. Incident photon to current efficiency (IPCE) spectra were recorded using a 150 W xenon lamp (KHP-1, Bunko-Keiki, Japan) fitted with a monochromator (Cornerstone 260) as a monochromatic light source. IPCE photocurrents were recorded under short-circuit conditions using the Keithley 2400 source meter.

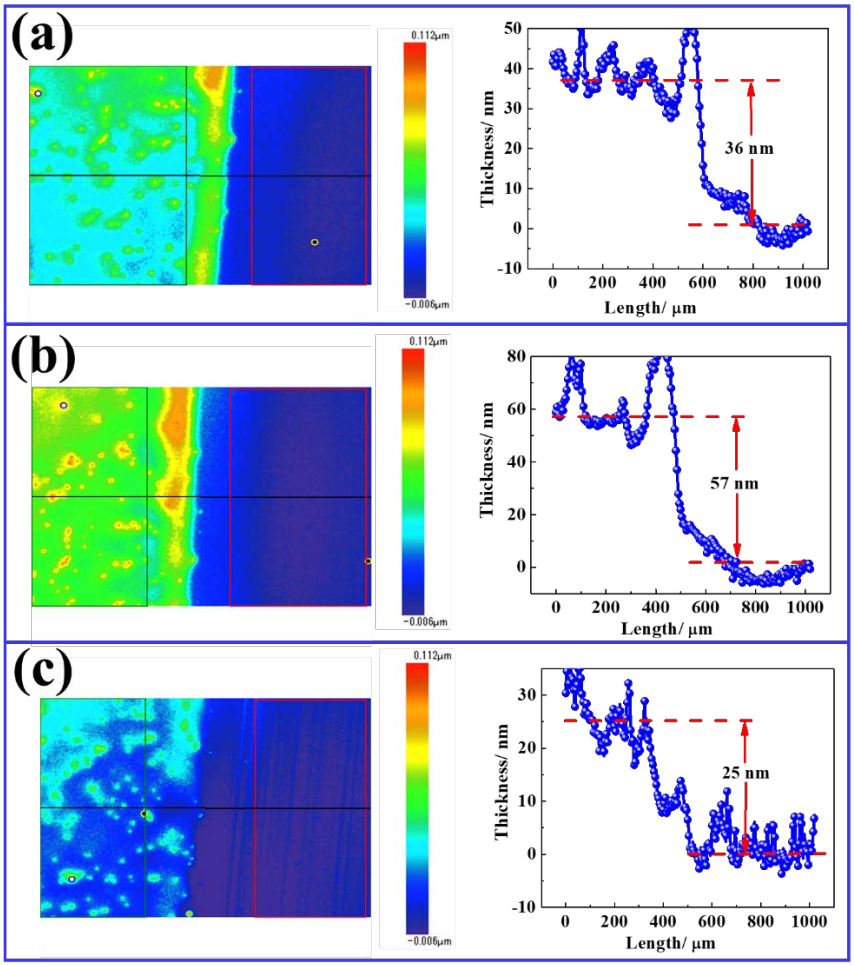

Fig. S1 Thickness of TiO_2 compact layer (c-TiO_2) on FTO glass. (a) 36 nm, (b) 57 nm, (c) 25 nm. The c-TiO_2 were prepared by spin-coating method, in detail 0.15 M titanium diisopropoxide bis (acetylacetonate) (75 wt% in isopropanol, Sigma-Aldrich) in 1-butanol (99.8%, Sigma-Aldrich) solution was spin-coated on an FTO substrate at 2000 rpm for 20 s, which was followed by heating on a hotplate at 125 °C for 5 min. Three samples were randomly selected with an average thickness of 39 nm ((36+57+25)/3=39 nm).

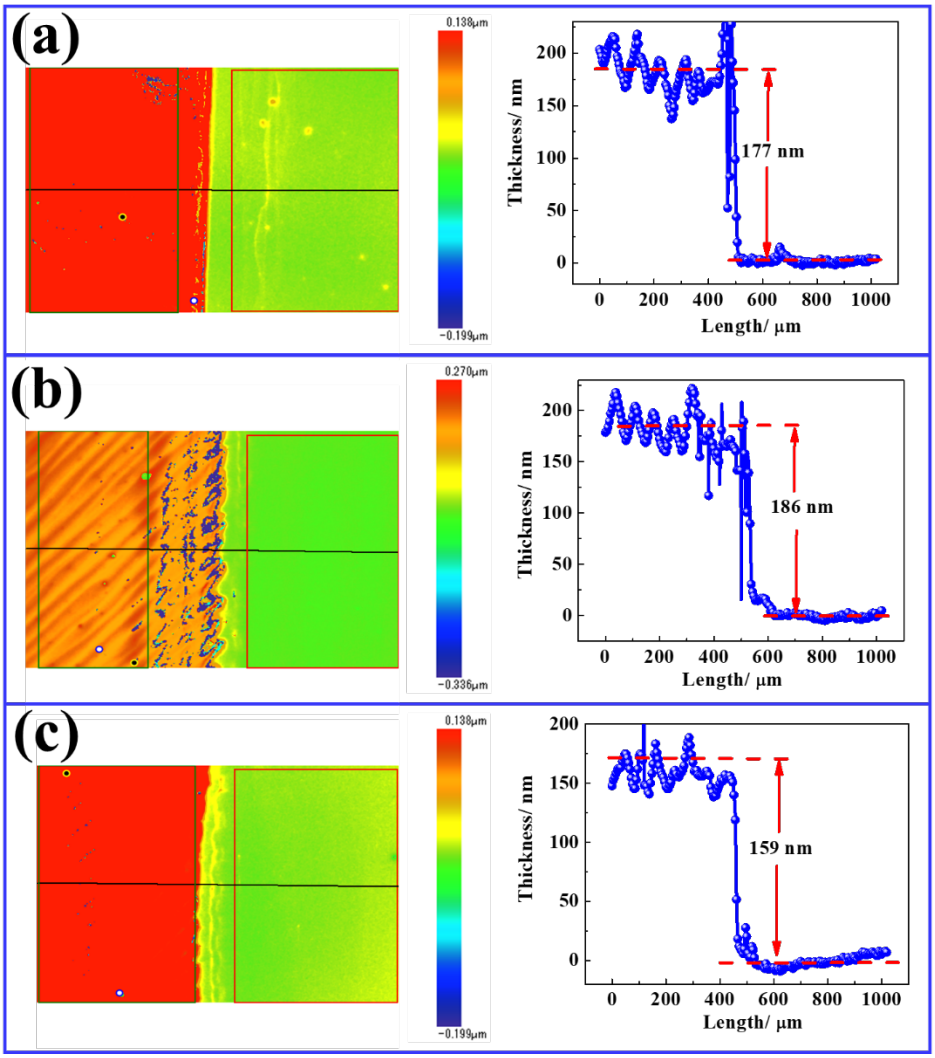

Fig. S2 Thickness of mesopourousTiO_2 layer (m-TiO_2) on FTO/c-TiO_2. (a) 177 nm, (b) 186 nm, (c) 159 nm. In detail the diluted-TiO_2 paste was spin-coated on the c-TiO_2 layer at 5000 rpm for 30 s, where the paste (Dyesol, 30 NR-D) was diluted in ethanol (TiO_2 paste/ethanol = 1/ 4, weight ratio). After drying on a hotplate at 125 °C for 5 min, the film was annealed at 500 °C for 1 h, providing m-TiO_2 with thickness of about 174 nm. Three samples were randomly selected. ((177+186+159)/3=174 nm).

Fig. S3 One-step anti-solvent method for preparing perovskite films. (a) Conventional process and (b) liquid nitrogen assist process, the ambient temperature is about 23 ℃ and the temperature during spin-coating was about 4 ℃.

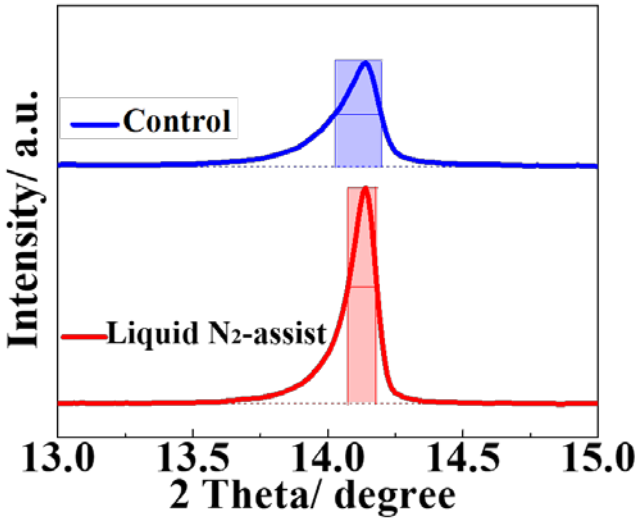

Fig. S4 X-ray diffraction spectra of $CH_3NH_3PbI_3$ perovskite films prepared by conventral process and liquid nitrogen assisted process. The full width at half maximum (FWHM) of peak at 14.17°。

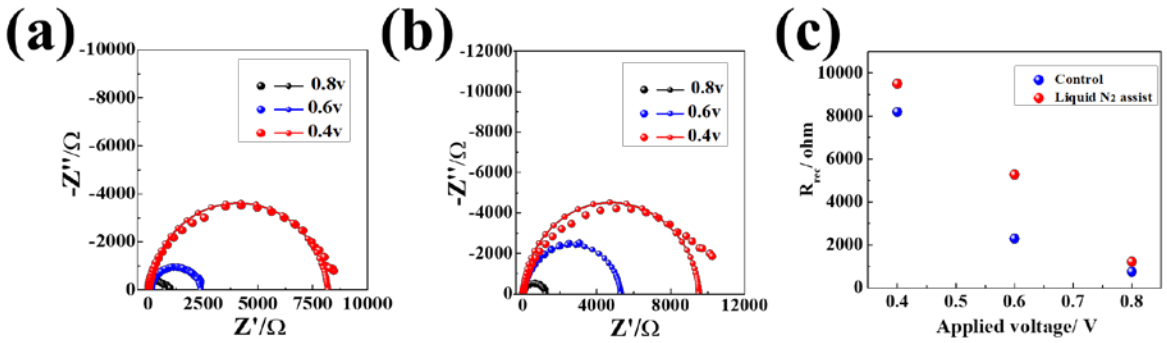

Fig. S5 Nyquist plots of perovskite solar cells based on $CH_3NH_3PbI_3$ measured in dark condition with different applied bias (0.4, 0.6 and 0.8 V). (a) Control group and (b) liquid nitrogen assisted group. (c) Charge recombination (Rrec) resistance extracted from EIS measurements at different applied bias.

Tab. S1. Photovoltaic parameters for thirty perovskite solar cells of control group.

Device #	J_{sc} /mAcm^{-2}	V_{oc} /V	FF	PCE /%
1	21.549	1.028	0.655	14.506
2	21.62	1.016	0.643	14.13
3	20.4	1.019	0.706	14.68
4	21.687	1.031	0.699	15.632
5	21.322	1.047	0.638	14.247
6	21.429	1.042	0.647	14.453
7	21.269	1.055	0.683	15.328
8	18.781	1.055	0.738	14.626
9	21.491	1.024	0.667	14.695
10	21.775	1.05	0.674	15.45
11	21.682	1.008	0.699	15.292
12	21.59	1.007	0.676	14.72
13	20.799	1.043	0.653	14.175
14	20.391	1.049	0.658	14.077
15	18.861	1.055	0.736	14.659
16	21.231	1.034	0.653	14.32
17	21.079	1.021	0.68	14.641
18	21.39	1.014	0.656	14.23
19	19.587	1.055	0.652	13.482
20	21.674	0.98	0.685	14.539
21	21.1	1.002	0.668	14.12
22	19.807	1.033	0.698	14.277
23	20.99	1.006	0.66	13.93
24	18.941	1.021	0.733	14.686
25	20.761	1.041	0.659	14.252
26	21.346	1.023	0.668	14.6
27	21.194	1.043	0.647	14.299
28	21.113	1.055	0.657	14.64
29	20.168	1.007	0.663	13.478
30	21.294	1.051	0.663	14.835
Average	20.877± 0.863	1.030± 0.019	0.673± 0.027	14.499± 0.488

Tab. S2. Photovoltaic parameters for thirty perovskite solar cells prepared by LN method.

Device #	J_{sc} /mAcm^{-2}	V_{oc} /V	FF	PCE /%
1	20.284	1.062	0.731	15.745
2	19.679	1.038	0.738	15.077
3	22.127	1.059	0.692	16.216
4	19.814	1.057	0.737	15.426
5	21.599	1.055	0.719	16.38
6	20.235	1.067	0.695	15.007
7	21.503	1.052	0.719	16.277
8	21.594	1.054	0.684	15.566
9	20.13	1.062	0.735	15.698
10	22.29	1.024	0.639	14.6
11	22.194	1.058	0.704	16.532
12	19.907	1.056	0.735	15.454
13	20.373	1.064	0.723	15.664
14	21.989	1.048	0.663	15.28
15	21.73	1.058	0.679	15.619
16	21.793	1.057	0.717	16.523
17	21.278	1.05	0.722	16.139
18	22.545	0.985	0.633	14.051
19	22.603	1.018	0.656	15.098
20	21.186	1.049	0.723	16.071
21	19.947	1.058	0.736	15.546
22	20.482	1.038	0.673	14.311
23	19.987	1.058	0.731	15.467
24	21.992	1.061	0.678	15.826
25	21.515	1.056	0.674	15.3
26	19.713	1.056	0.725	15.102
27	20.549	1.069	0.722	15.852
28	21.148	1.087	0.692	15.911
29	22.752	1.037	0.648	15.288
30	21.816	1.039	0.665	15.071
Average	21.158± 0.959	1.051± 0.018	0.700± 0.032	15.536± 0.595